Noonan and LEOPARD syndrome Shp2 variants induce heart displacement defects in zebrafish

Monica Bonetti[1], Jeroen Paardekooper Overman[1], Federico Tessadori[1], Emily Noël[1], Jeroen Bakkers[1] and Jeroen den Hertog[1,2]

1 Hubrecht Institute-KNAW and University Medical Center Utrecht, 3584 CT Utrecht, The Netherlands
2 Institute of Biology 2333 CC, Leiden, The Netherlands

Development 2014, May; 141(9):1961-1970

Abstract

Germline mutations in *PTPN11*, encoding Shp2, cause Noonan syndrome (NS) and LEOPARD syndrome (LS), two developmental disorders that are characterized by multiple overlapping symptoms. Interestingly, Shp2 catalytic activity is enhanced by NS mutations and reduced by LS mutations. Defective cardiac development is a prominent symptom of both NS and LS, but how the Shp2 variants affect cardiac development is unclear. Here, we expressed the most common NS and LS Shp2-variants in zebrafish embryos to investigate their role in cardiac development in vivo. Heart function was impaired in embryos expressing NS and LS variants of Shp2. The cardiac anomalies first occurred during elongation of the heart tube and consisted of reduced cardiomyocyte migration, coupled with impaired leftward heart displacement. Expression of specific laterality markers was randomized in embryos expressing NS and LS variants of Shp2. Ciliogenesis and cilia function in Kupffer's vesicle was impaired, likely accounting for the left/right asymmetry defects. Mitogen activated protein kinase (MAPK) signaling was activated to a similar extent in embryos expressing NS and LS Shp2-variants. Interestingly, inhibition of MAPK signaling prior to gastrulation rescued cilia length and heart laterality defects. These results suggest that NS and LS Shp2-variant mediated hyperactivation of MAPK signaling leads to impaired cilia function in Kupffer's vesicle, causing left-right asymmetry defects and defective early cardiac development.

Introduction

PTPN11 encodes Shp2, a ubiquitously expressed non-receptor protein-tyrosine phosphatase (PTP) with two Src homology 2 (SH2) domains [1-3], that is involved in a variety of signal transduction processes, such as the Ras-Raf-MAP kinase [4], Jak-Stat [2,5], and Phosphatidylinositol-3 kinase (PI-3K) pathways [6]. Shp2 plays a critical role in the transduction of the signal from Receptor Tyrosine Kinases (RTKs), including the receptors of platelet-derived growth factor (PDGFR) [7], fibroblast growth factor (FGFR) [8] and the epidermal growth factor (EGFR) [9,10] as well as from cytokine receptors and Integrins [8,9].

Missense germline mutations in *PTPN11* are associated with Noonan syndrome (NS) (OMIM: 163950) and LEOPARD syndrome (LS) (OMIM: 151100), two autosomal dominant disorders. NS is a relatively common disorder that affects 1 in 1,000-2,000 live births. NS patients are characterized by congenital heart defects, including atrial and ventricular septal defects, pulmonary stenosis and hypertrophic cardiomyopathy (HCM) [11,12]. In addition, NS patients display short stature and facial abnormalities. LS is a more rare disorder (1:3,500 live births) that shows a substantial overlap with the various symptoms of NS patients with two more clinical manifestations that are specific for LS patients: deafness and "café-au-lait" spots on the skin [13,14]. The congenital heart defects among patients with *PTPN11* mutations differ between NS and LS patients, in that pulmonary stenosis is most common in NS, while HCM prevails in LS patients [15,16].

Interestingly, the biochemical properties of NS-Shp2 and LS-Shp2 are distinct, in that NS mutations enhance catalytic activity and LS mutations strongly reduce PTP activity [17,18]. The crystal structure of Shp2 shows that in the absence of a binding partner, the N-SH2 domain interacts with the PTP domain and blocks the catalytic site [19]. NS mutations predominantly reside in the interface between the N-SH2 domain and the PTP domain, resulting in the disruption of the closed conformation and enhanced catalytic activity of NS-Shp2 [17,20]. In contrast, most LS mutations reside close to the active site and result in strongly reduced, yet detectable catalytic activity [17,21,22]. How two mutations with opposite effects on catalytic activity result in syndromes with similar clinical symptoms is a conundrum that still needs to be resolved.

NS-Shp2 causes up-regulation of the MAPK pathway [6]. Whereas several studies show that LS mutations down-regulate the level of phosphorylated ERK [18,23], the role of LS-Shp2 mutation on the MAPK pathway is still controversial [24-26]. Increased RAS/MAPK signaling is implicated in the gain-of-function phenotypes that are caused by expression of the LS *Drosophila* orthologue of *PTPN11*, *corkscrew* (*csw*) [26], suggesting a mechanism by which NS and LS variants may result in similar phenotypes. However, NS- and LS-signaling is distinct, because it is well established that LS-mutations, but not NS mutations [27], enhance PI3K/AKT signaling in hearts of LS/+ knock-in mice [18] as well as in fibroblasts isolated from LS patients [24]. The similarities in RAS/MAPK signaling of NS and LS variants may underlie the overlapping symptoms in NS and LS, whereas the differences in PI3K/Akt signaling may cause the differences in NS- and LS-induced developmental defects.

Shp2 knock-out, knock-down and gain-of function studies in a variety of organisms have begun to reveal the roles of Shp2 in embryonic development. Shp2 null mouse embryos die pre-implantation due to defective Erk activation and trophoblast stem cell death [28]. Dominant-negative Shp2 mutants disrupt gastrulation in *Xenopus* [29]. Moreover, mouse models have been generated for

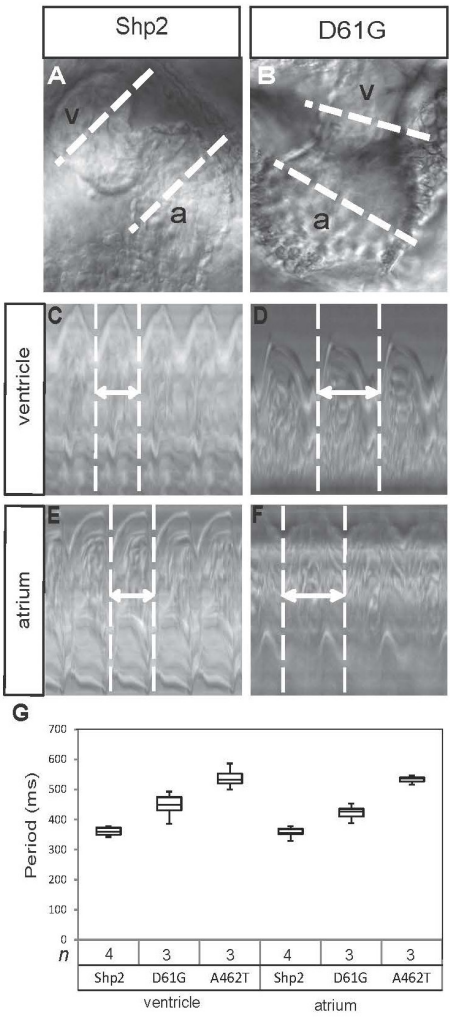

Figure 1. Impaired cardiac function in embryos expressing Shp2-D61G and Shp2-A462T. (A-B) The hearts of WT-Shp2 (Shp2) and Shp2-D61G expressing zebrafish embryos were imaged by high speed video recording microscopy at 2 dpf. White dotted lines through the atrium (a) and the ventricle (v) are indicated. (C-F) Ventricular (C,D) and atrial (E,F) kymographs from 2 dpf embryonic hearts. Note the longer period of the Shp2-D61G expressing heart, compared to the WT-Shp2 expressing heart (double arrow and white dotted vertical lines). (G) Quantitative analysis of the heart period in the ventricle or atrium of WT-Shp2, Shp2-D61G and Shp2-A462T expressing embryos. Whisker plots are depicted.

the two most prevalent NS and LS mutations, *Ptpn11*$^{D61G/+}$ and *Ptpn11*$^{Y279C/+}$, respectively. These mice exhibit developmental defects, including reduced length, cranio-facial abnormalities and congenital heart defects, reminiscent of the clinical characteristics of the human disorders [30,31]. In particular pulmonary stenosis and HCM are evident in the NS and LS mice, respectively. Shp2 is conserved in zebrafish and we previously generated the most common human NS and LS mutations in a cDNA encoding full length zebrafish Shp2. Micro-injection of mRNA encoding mutant Shp2 variants into zebrafish embryos at the one-cell stage induces gastrulation cell movement defects as well as craniofacial and cardiac defects [32]. Furthermore, Stewart *et al.* used zebrafish embryos to show that the function of Shp2 in neural crest cells underlies LS pathogenesis [23].

The role of NS and LS Shp2 variants in the development of cardiac defects is still unclear. Zebrafish has become a powerful model to study cardiac development in recent years [33,34]. We set out to study early heart development in zebrafish embryos expressing NS and LS variants of Shp2, taking advantage of the transparency of zebrafish embryos, which facilitates time-lapse analysis of the onset and nature of the cardiac defects *in vivo*. Our analyses revealed impaired heart function and morphogenesis, which were highly similar in NS- and LS-Shp2 expressing embryos. Furthermore, the heart defects were accompanied by randomization of left-right asymmetry, which was likely due to impaired ciliogenesis and defective cilia function in Kupffer's vesicle that we observed in early embryos. Treatment with a MEK-inhibitor, CI-1040, prior to gastrulation rescued defective leftward heart displacement and the laterality defects in NS- and LS-Shp2 expressing embryos. Taken together, our results provide insight into the mechanism by which NS and LS Shp2-variants induced laterality defects through hyperactivation of MAPK signaling, resulting in cardiac defects during early development.

Results

Expression of NS and LS Shp2-variants caused defects in cardiac function

To investigate the role of Shp2 variants in cardiac function, Shp2-D61G and Shp2-A462T mRNAs were injected at the 1-cell stage. In order to monitor expression of mutant Shp2, we fused a green fluorescent protein (GFP)-peptide 2A sequence to the NH2-terminus of Shp2, which is cleaved off autoproteolytically [35] (Supplemental Figure 1). Following expression of (mutant) Shp2, the developing heart was analyzed at 55 hpf by high-speed video recording. Kymographs of the atrium and ventricle were generated, allowing quantification of heart function as described before [36]. Representative examples of kymographs of embryos expressing WT-Shp2 and Shp2-D61G are depicted (Figure 1A-F). Quantification of the kymographs of WT-Shp2, Shp2-D61G and Shp2-A462T injected embryos revealed significantly longer cardiac cycles in the Shp2-variant expressing embryos, reflecting a reduced but regular heart rate (Figure 1G). Other functional defects, such as an atrio-ventricular block or uncoupling of the two chambers were not detected in Shp2-D61G and Shp2-A462T expressing embryos. These results illustrate functional cardiac defects, particularly a reduced heart rate, in embryos expressing NS and LS variants of Shp2.

Impaired heart asymmetry in embryos expressing NS and LS Shp2-variants

To further characterize the cardiac phenotype in response to expressing of NS and LS variants of Shp2, we first examined the overall morphology and regionalization of the heart at 55 hpf by *in situ* hybridization (ISH), using a panel of cardiac markers. At this stage, the heart chambers are completely formed in wild type embryos and the heart undergoes looping morphogenesis. Analysis of heart shape using a *myl7*-specific probe (formerly known as *cmlc2*) revealed that the hearts of Shp2-D61G and Shp2-A462T expressing embryos exhibited either inverted looping (14%

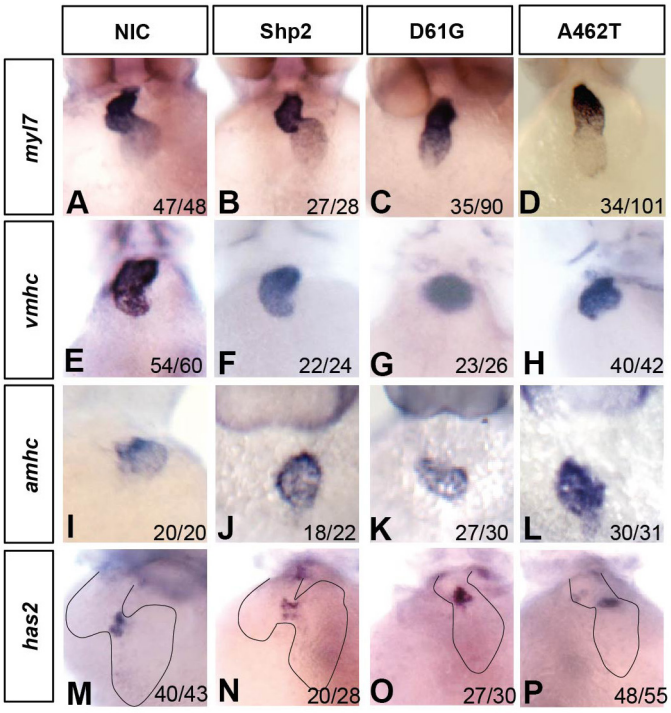

Figure 2. Heart defects in embryos expressing Shp2-D61G and Shp2-A462T. Non-injected control embryos (NIC) and embryos injected at the one-cell stage with mRNA encoding WT-Shp2 (Shp2), Shp2-D61G, or Shp2-A462T were fixed at 48 hpf and *in situ* hybridization was performed using probes for the myosin genes *myl7* (A-D, cardiomyocytes), *vmhc* (E-H, ventricle), *amhc* (I-L, atrium), and for *has2* (M-P, endocardial cushions). Representative pictures are shown and the number of embryos showing this pattern as well as the total number of embryos that were analyzed is indicated in the bottom right corner of each panel. The outline of the heart is indicated with a dashed line in panels M-P.

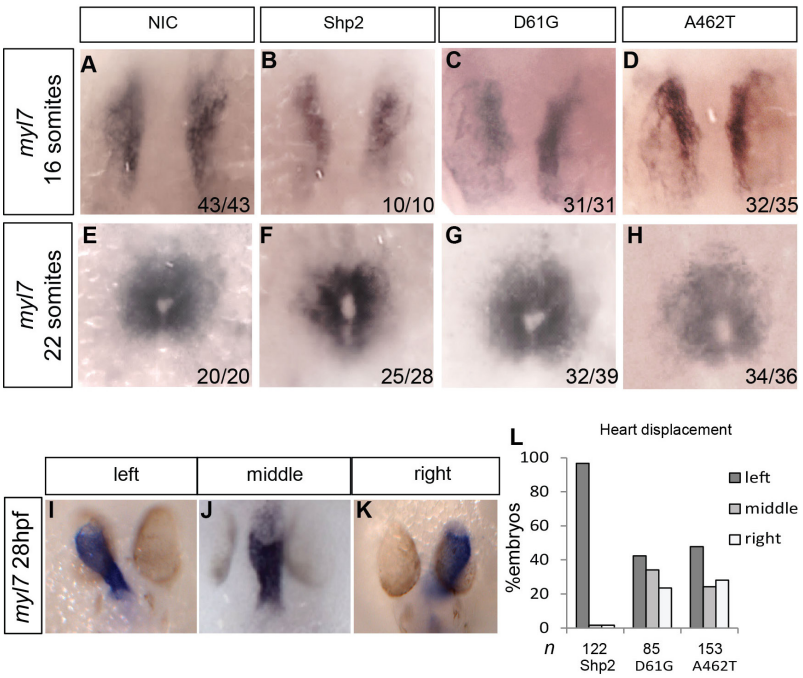

Figure 3. Randomized heart displacement in response to expression of Shp2-D61G and Shp2-A462T. Embryos were injected at the one-cell stage with mRNA encoding WT-Shp2, Shp2-D61G or Shp2-A462T and fixed at the 16-somite stage, the 22-somite stage or at 28 hpf. *In situ* hybridization was done using a *myl7*-specific probe to mark cardiomyocytes. (A-H) The ratio of the number of embryos displaying the depicted pattern and the total number of embryos that were analyzed for each condition is indicated in the bottom right of each panel. (I-K) Representative pictures are shown displaying heart displacement to the left (I), middle (J) and right (K). (L) Percentages of left, middle and right cardiac displacement are depicted.

and 11%, respectively) or non-looped heart (39% and 25%, respectively) in contrast to non-injected control and WT-Shp2 injected embryos, (Figure 2A-D). Myocardial chamber specification was not affected in NS-Shp2 and LS-Shp2 injected embryos as determined by expression of ventricular myosin heavy chain (*vmhc*) (Figure 2E-H) and atrium myosin heavy chain (*amhc*) (Figure 2I-L). Next, the formation of the endocardial cushions, from which the atrioventriclar valves will develop, was assessed by *has2* expression. In Shp2-D61G and Shp2-A462T expressing embryos, *has2* expression was not affected, compared to non-injected control and WT-Shp2 expressing embryos (Figure 2M-P). Expression of this panel of markers was also assessed in embryos expressing Shp2-T73I (NS) and Shp2-G465A (LS) with similar results (Supplemental Figure 2), indicating that all NS and LS variants induced similar defects. Taken together, these data indicate that expression of NS- and LS-variants of Shp2 led to a failure to undergo heart looping in a large proportion of the embryos without inducing defects in cardiac chamber specification or endocardial cushion formation. In addition, the NS- and LS-variants of Shp2 induced cardiac defects to a similar extent during early development.

To investigate at which stage the cardiac defects arise in embryos expressing NS and LS variants of Shp2, *myl7* expression was analyzed at different time points of heart development, particularly during cardiac fusion and heart tube elongation. Zebrafish heart formation is initiated by fusion

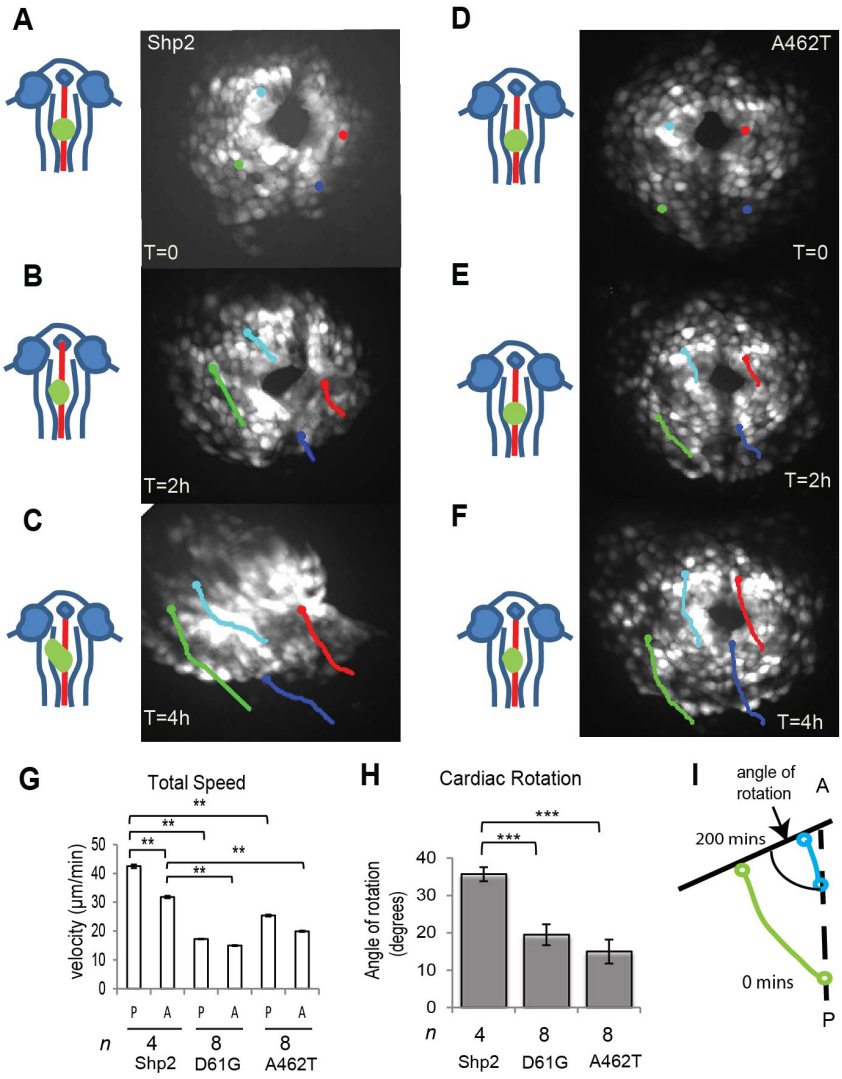

Figure 4. Impaired cardiomyocyte migration in embryos expressing Shp2-D61G and Shp2-A462T. Embryos from the *tg(myl7:GFP)* line were injected with mRNA encoding WT-Shp2, Shp2-D61G or Shp2-A462T lacking eGFP-peptide 2A sequences to allow imaging of GFP-positive cardiomyocytes from the 22-somite stage onwards. **(A-F)** Representative individual GFP-positive cells were color-coded according to their location within the cardiac field at the 22-somite stage and tracked over a 200 min period. The resulting cell tracks are indicated. Dorsal view with the anterior to the top. Schematic representations of the embryos on the left indicate the position and shape of the heart in green. (A-C) WT-Shp2; (D-F) Shp2-A462T **(G)** Quantification of the total speed of posterior (P) and anterior (A) cardiac progenitor cells. Following imaging, heart displacement was assessed in the embryos. WT-Shp2 expressing embryos displayed normal leftward heart displacement; embryos expressing Shp2-D61G and Shp2-A462T that did not display normal heart displacement were selected for further analysis. **(H)** Clockwise cardiomyocyte rotation was determined of the same embryos as in (G). Rotation was quantified as depicted in (I). In (G) and (H), averages are indicated and error bars indicate standard error of the mean. Statistical significance was determined using Student's t-test and is indicated with **, $p < 0.01$ and ***, $p<0.001$.

of two bilateral pools of cardiomyocytes at the 16-somite stage (16 hpf) into a cardiac disc at the midline of the embryo at 22 somites (20 hpf) [33,37]. No obvious defects were detected in *myl7* expression or cardiac fusion between non-injected control, WT-Shp2, Shp2-D61G and Shp2-A462T expressing embryos up to 22 somites (Fig 3A-H). At 28 hpf, the heart in WT-Shp2 expressing embryos formed a tube that extended from the midline to the area under the left eye (Figure 3I), which resembled normal heart displacement. In contrast, in Shp2-D61G and Shp2-A462T expressing embryos the displacement of the heart is randomized: 23% of Shp2-D61G expressing embryos and 28% of Shp2-A462T expressing embryos showed the heart on the right, while 34% of Shp2-D61G expressing embryos and 24% of Shp2-A462T expressing embryos displayed positioning of the heart tube at the midline (Figure 3J-L). Taken together, these results indicate that the first signs of cardiac abnormality in embryos expressing Shp2 variants are observed during asymmetric displacement of the heart tube.

Decreased cardiomyocyte migration speed and rotation in embryos expressing NS and LS Shp2-variants

Randomization of heart displacement may be caused by compromized cardiomyocyte migration [38]. *Tg(myl7:GFP)* embryos express eGFP in cardiomyocytes and were used for high-resolution confocal time-lapse imaging to assess cardiomyocyte migration. Since WT-Shp2 expressing embryos were indistinguishable from non-injected control embryos in *in situ* hybridization experiments (Figure 2, 3), we used WT-Shp2 expressing embryos as a control for the embryos expressing NS and LS variants of Shp2 from here on after. Single cells were tracked in WT-Shp2, Shp2-D61G and Shp2-A462T expressing embryos from cardiac disc stage (21 somites, 19.5 hpf) for 4 hours and their velocities and directions were determined. Consistent with observations of heart morphogenesis in wild type embryos [39,40], cardiac cells moved towards the left and anterior part of the embryo in WT-Shp2 expressing embryos (n=4). Cardiomyocytes in the posterior part of the cardiac disc moved faster than anterior cells (Figure 4A-C). The Shp2-D61G and Shp2-A462T expressing embryos were imaged at 19.5 hpf, like the WT-Shp2 expressing embryos and subsequently, heart displacement was assessed at 24 hpf, allowing correlation between early migration defects and heart displacement. Embryos that displayed impaired heart displacement were selected for further analysis. It is noteworthy that none of the selected embryos displayed heart displacement to the right (Shp2-D61G, n=8; Shp2-A462T, n=8), which may be due to low penetrance of rightward heart displacement. Although cardiomyocytes in the selected embryos formed a cardiac tube, they showed reduced migration to the left. Representative images of an embryo expressing Shp2-A462T are depicted in Figure 4D-F. Quantification of the speed of cardiomyocytes confirmed slower migration of cells in embryos expressing Shp2-D61G and Shp2-A462T, compared to WT-Shp2 (Figure 4G). Cardiomyocytes in selected embryos expressing Shp2-D61G and Shp2-A462T did not cross the midline, but instead migrated anteriorly, which is consistent with defective heart displacement to the left. Rotation of the heart tube was quantified as described before and the observed 30° clockwise rotation of the cardiac cone in WT-Shp2 expressing embryos was consistent with the previously reported clockwise rotation in control embryos [39]. Clockwise rotation was significantly decreased in embryos expressing Shp2-D61G and Shp2-A462T with impaired leftward heart displacement, compared to control WT-Shp2 (Figure 4H). Our results indicate that directional cardiomyocyte migration and heart tube rotation is reduced in embryos expressing NS and LS Shp2-variants, which is consistent with the observed defects in heart tube displacement.

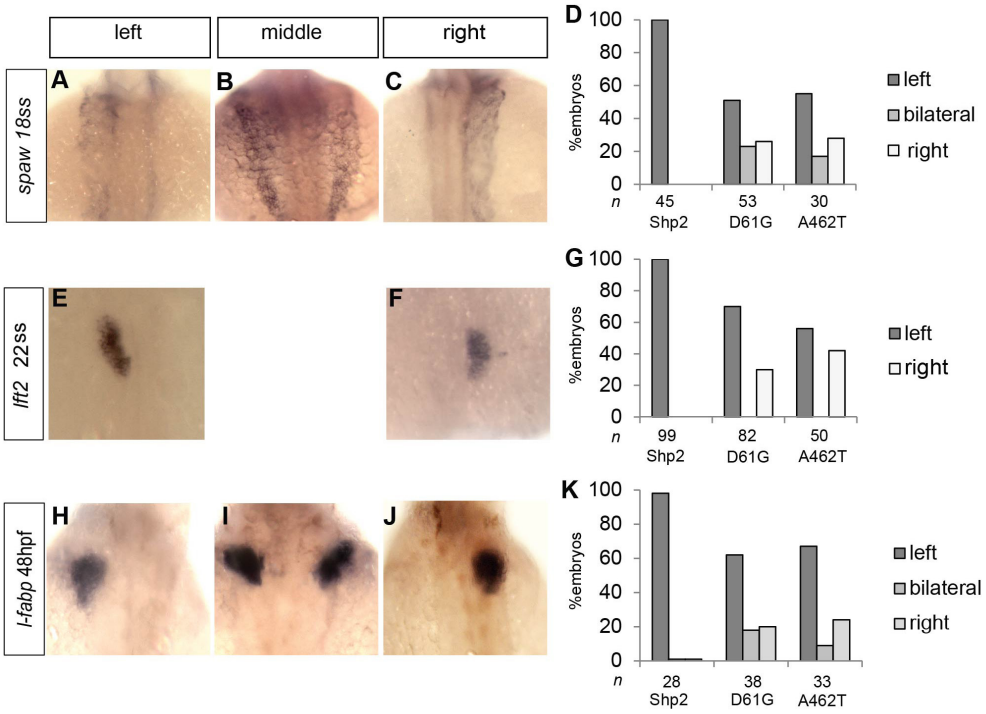

Figure 5. Expression of Shp2-D61G and Shp2-A462T induced L/R asymmetry defects. Embryos were injected at the one-cell stage with mRNA encoding WT-Shp2 (Shp2), Shp2-D61G or Shp2-A462T and fixed at the stage indicated in the panel. *In situ* hybridization was done using probes specific for *spaw* (A-D, *southpaw*), *lft2* (E-G, *lefty2*), and *fabp* (H-K, fatty acid binding protein, marking the liver). Representative pictures are shown of Shp2-D61G expressing embryos. Note that *lft2* expression was only observed on the left side or on the right side. Organ asymmetry as assessed using the different markers was scored for embryos injected with WT-Shp2, Shp2-D61G and Shp2-A462T. Percentages of left, middle/bilateral and right expression of the markers are depicted.

NS and LS Shp2-variants disrupt left/right asymmetry

To determine if the loss of asymmetry in the hearts of embryos expressing NS and LS Shp2-variants is associated with disruption of overall L/R asymmetry, we analyzed the expression of a number of laterality markers. *Southpaw* (*spaw*) is one of the earliest markers displaying asymmetric expression in development [41]. *Spaw* was predominantly expressed in the left lateral plate mesoderm (LPM) in WT-Shp2 expressing embryos (Figure 5A). *Spaw* expression was affected in embryos expressing Shp2-D61G and Shp2-A462T, compared to WT-Shp2, in that 23% of Shp2-D61G and 17% of Shp2-A462T expressing embryos displayed bilateral *spaw* expression and 26% of Shp2-D61G and 28% of Shp2-A462T expressing embryos expressed *spaw* exclusively in the right LPM (Figure 5B-D). Next, expression of *Lefty2* (*lft2*), a downstream target of *spaw,* was investigated at the 22 somite stage (20 hpf). In WT-Shp2 expressing embryos, *lft2* was detected in the left cardiac field in all cases (Figure 5E). In contrast, expression of *lft2* in Shp2-D61G and Shp2-A462T expressing embryos was randomized. 30% of the Shp2-D61G expressing embryos expressed *lft2* on the right side (Figure 5E-G). Similarly, in Shp2-A462T expressing embryos, *lft2* expression was detected at the right side in 42% of the embryos. *Southpaw* is required for visceral organ L/R asymmetry [41], suggesting that defects in L/R asymmetry may not be limited to the heart in embryos expressing Shp2 variants. To investigate this, the position of the liver was

assessed by analysis of the expression of *fabp*. *Fabp* expression was randomized at 48 hpf in embryos expressing Shp2-D61G and Shp2-A462T, in that the liver developed on the opposite side in 20% of the Shp2-D61G expressing embryos and 24% of the Shp2-A462T expressing embryos, or on both sides in 18% of the Shp2-D61G and 9% of the Shp2-A462T expressing embryos (Figure 5H-K). In control WT-Shp2 expressing embryos, the liver always developed on the left side of the embryos. Analysis of the embryonic midline using the sonic hedgehog marker [42] indicated that expression of Shp2-D61G and Shp2-A462T altered left-right patterning without disrupting the

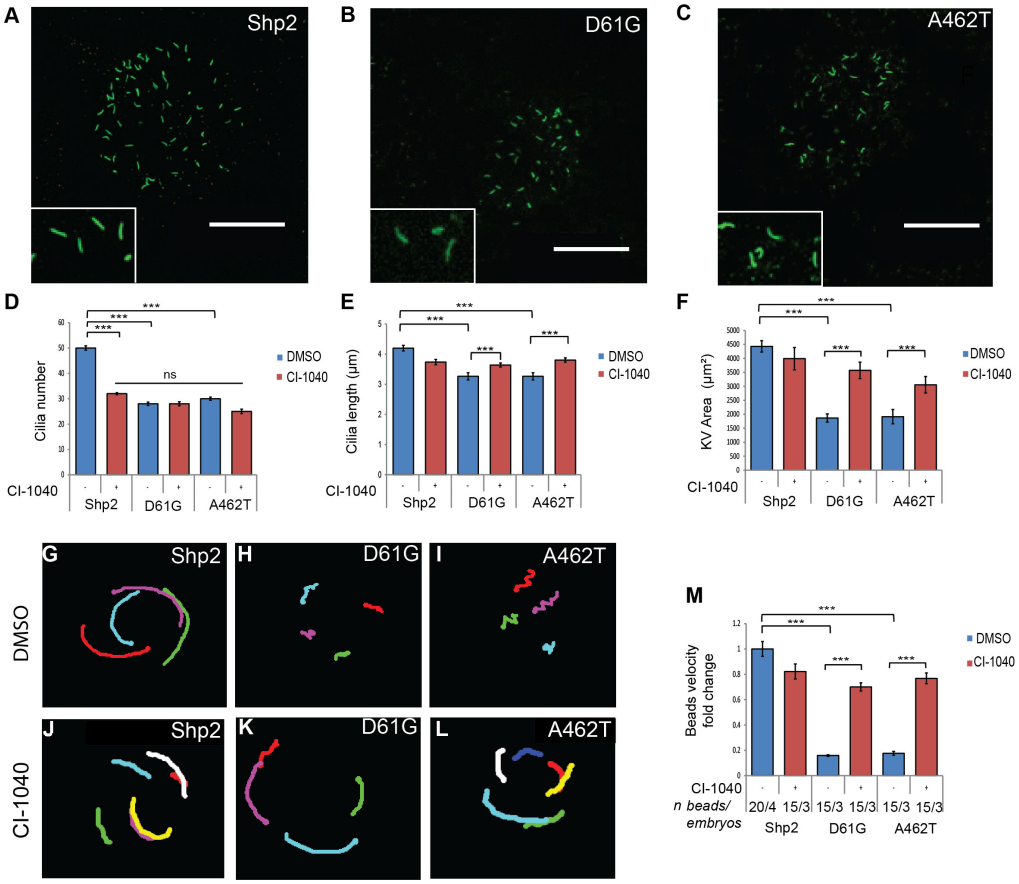

Figure 6. Impaired ciliogenesis and cilia function in Kupffer's vesicle in embryos expressing Shp2-D61G and Shp2-A462T. (A-C) Immunohistochemistry was done using anti-acetylated tubulin on WT-Shp2, Shp2-D61G or Shp2-A462T expressing embryos that were fixed at the 10-somite stage. Representative confocal images are depicted here. Scale bar indicates 50 µm. (D-F) Quantification of the cilia number, cilia length and KV area in WT-Shp2, Shp2-D61G and Shp2-A462T expressing embryos that were treated with 0.5% DMSO (control) or 0.25 µM CI-1040 at 4.5 hpf for 1 h and fixed at the 10-somite stage (n=10 for each condition). Averages are depicted with error bars indicating standard error of the mean. Statistical significance was determined using Student's t-test: ***, $p<0.001$; **, $p<0.01$. (G-L) Tracks of fluorescent beads injected in KV. (G–L) Maximum projections of fluorescent bead movements injected in the KV of WT-Shp2, Shp2-D61G or Shp2-A462T expressing embryo, respectively that were treated with 0.5% DMSO or 0.25 µM CI-1040 at 4.5 hpf for 1 h and fixed at the 10-somite stage. (M) Average flow velocity of beads in KV of embryos expressing WT-Shp2, Shp2-D61G and Shp2-A462T for the DMSO treatment and for the CI-1040 treatment. Averages are depicted with error bars indicating standard error of the mean. Statistical significance was determined using Student's t-test: ***, $p<0.001$.

midline that provides a barrier between the left and the right side (Supplemental Figure 4). These results show that L/R patterning in the LPM is impaired in embryos expressing NS and LS Shp2-variants, which may lead to randomization of heart and gut laterality.

Ciliogenesis and cilia function in Kupffer's vesicle are impaired in embryos expressing NS and LS Shp2-variants

It is well established that Kupffer's vesicle (KV), a fluid-filled ciliated organ, is involved in the establishment of L/R asymmetry in zebrafish [43,44]. Through the oriented rotation of the cilia inside the KV, asymmetric expression of genes such as *spaw* and *lft2* is established. Immunohistochemistry was done using an acetylated tubulin antibody to detect cilia in the KV of 10 somite-stage embryos (14 hpf) (Figure 6A-C). The mean number of cilia was 51.4 ± 0.5 in WT-Shp2 expressing embryos, whereas in embryos expressing Shp2-D61G and Shp2-A462T, the number of cilia was significantly reduced to 30.4 ± 0.7 and 28.5 ± 0.4, respectively (n=10 embryos each) (Figure 6D). Also, the cilia length was significantly reduced in embryos expressing NS and LS Shp2-variants (both 3.2 µm ± 0.1, n cilia=241 for Shp2-D61G and n cilia=172 for Shp2-A462T, respectively) compared to control (4.2 ± 0.1 µm, n cilia=379 for WT-Shp2) (Figure 6E). Measurements of the area of KV indicated significant differences in lumen size among wild-type (4517 ± 355 μm^2, n=10), Shp2-D61G (2243 ± 190 μm^2, n=10) and Shp2-A462T (1914 ± 256 μm^2, n=10) embryos (Figure 6F). These results suggest that disruption of L/R asymmetry in embryos expressing NS and LS variants of Shp2 was a consequence of defective KV function, resulting from impaired ciliogenesis in the KV. To determine the KV functionality directly, we analyzed the fluid flow in embryos expressing NS and LS variants of Shp2. Tracking of fluorescent beads injected into the KV lumen of wild-type Shp2 expressing embryos showed counterclockwise rotation of the beads (Fig 6G). By contrast, tracking of the beads in Shp2-D61G and Shp2-A462T expressing embryos showed that the beads moved about randomly (Fig6 H-I), indicating a loss of coordinated flow. In addition, beads tracked in Shp2-D61G and Shp2-A462T expressing embryos showed a strongly reduced average flow velocity relative to wild-type Shp2 expressing embryos (Figure 6M). These results indicate that ciliogenesis and cilia function is impaired in the KV of embryos expressing NS and LS variants of Shp2, resulting in defective KV function.

Early treatment with the MEK-inhibitor, CI-1040, rescued L/R asymmetry, heart asymmetry and KV function in embryos expressing NS and LS Shp2-variants

Shp2 variants enhance RAS/MAPK signaling [6]. Previously, we and others showed that inhibition of MEK rescued developmental defects in zebrafish embryos that were caused by expression of activators of the RAS/MAPK pathway [45,46]. We investigated whether inhibition of MEK would also rescue the cardiac defects in embryos expressing NS and LS Shp2-variants. First, the efficacy of the MEK inhibitor, CI-1040, to rescue early developmental defects was assessed. Expression of Shp2-D61G or Shp2-A462T in zebrafish embryos induced cell movement defects, resulting in elongated embryos at bud stage (10 hpf) (Figure 7A-C). Treatment with 0.25 µM CI-1040 at 4.5 hpf for 1 h rescued development at 10.5 hpf of embryos expressing Shp2-D61G and Shp2-A462T (Figure 7D-F). Quantification of the epiboly defects confirmed the rescue of the embryos expressing NS and LS Shp2-variants (Figure 7G). In addition, we confirmed that elevated pERK levels in embryos expressing Shp2-D61G and Shp2-A462T were reduced by CI-1040-mediated inhibition of MEK at 10 hpf (Figure 7H).

Next, the effect of CI-1040 treatment was assessed on asymmetry of the heart in embryos expressing Shp2-D61G and Shp2-A462T. Treatment with 0.25 µM CI-1040 at 4.5 hpf for 1 h rescued

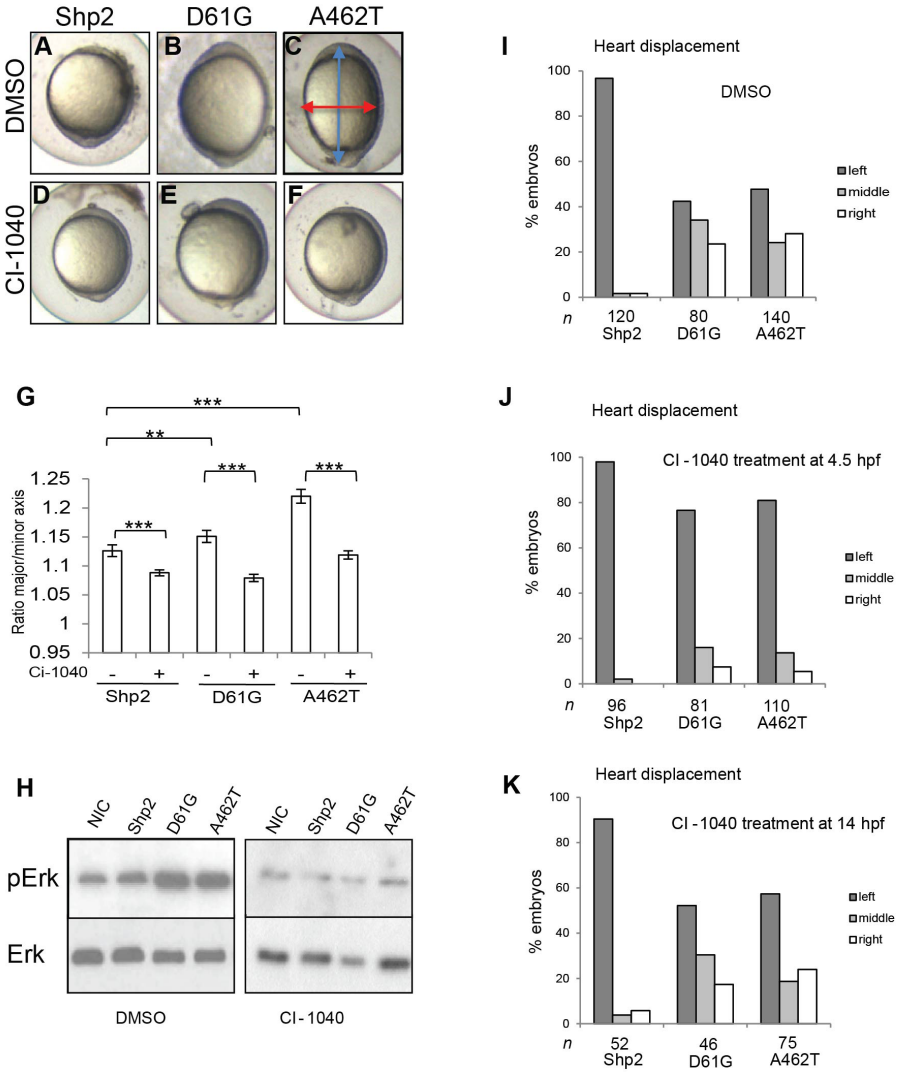

Figure 7. Early treatment with the MEK-inhibitor CI-1040 rescued leftward heart displacement and cilia length in embryos expressing NS and LS Shp2-variants. Embryos were injected with mRNA encoding WT-Shp2 (Shp2), Shp2-D61G and Shp2-A462T at the one cell stage. **(A-F)** Representative images of bud stage embryos are depicted. The shape of the NS- and LS-Shp2 expressing embryos is restored by treatment with 0.25 µM CI-1040 at 4.5 hpf for 1h. **(G)** The ratio between the length of the major and minor axis was determined as quantitative measure of the epiboly defects in NS- and LS-Shp2 expressing embryos. Averages are depicted with error bars indicating standard error of the mean. Statistical significance was determined using Student's t-test (**, p<0.01; ***, p<0.001). **(H)** Embryos were treated with MEK inhibitor CI-1040 (0.25 µM) for 1 h at 4.5 hpf or mock-treated with DMSO and lysed at 10 hpf. Immunoblots of the zebrafish lysates were stained using antibodies specific for pErk and Erk. The experiment was repeated three times and representative blots are depicted here. **(I-K)** Embryos were mock-treated with DMSO (I) or with CI-1040 for 1h at 4.5 hpf (J) or at 10 hpf (K). Heart displacement was determined in embryos following in situ hybridization with a myl7-specific probe as in Figure 4. Histograms represent the percentage of embryos with heart displacement to the left, middle or right.

leftward displacement of the heart at 24 hpf of Shp2-D61G and Shp2-A462T expressing embryos (Figure 7I,J). However, treatment of these embryos for 1 h with CI-1040 at the 10-somites stage (14 hpf) did not restore normal heart displacement in embryos expressing NS and LS Shp2-variants (Figure 7K). Treatment with 0.25 μM CI-1040 at 4.5 hpf for 1 h largely rescued randomization of the left-right asymmetry markers and of the liver (Supplemental Figure 5). These results indicate that inhibition of MEK at early stages rescues L/R asymmetry in embryos expressing NS and LS Shp2-variants.

Finally, the effect of CI-1040 treatment on ciliogenesis and cilia function in KV was assessed. The cilia number was not rescued upon treatment with 0.25 μM CI-1040 at 4.5 hpf for 1 h. In fact, the cilia number in CI-1040-treated WT-Shp2 expressing embryos was significantly reduced to similar levels as in CI-1040 treated embryos expressing NS or LS variants of Shp2 (Figure 6D). Yet, CI-1040 treatment rescued cilia length in embryos expressing Shp2 variants (3.6 ± 0.1 μm in Shp2-D61G and 3.8 ± 0.1 μm in Shp2-A462T expressing embryos, compared to 3.2 ± 0.1 μm in untreated embryos) (cf. Figure 6E). Cilia length in WT-Shp2 expressing embryos was reduced somewhat in response to CI-1040 treatment (from 4.2 ± 0.1 μm to 3.7 ± 0.1 μm; cf. Figure 6E,) and hence, CI-1040 treatment abolished the difference in cilia length between embryos expressing WT-Shp2 and Shp2 variants. Moreover, CI-1040 treatment rescued KV area (3736 ± 373 μm^2 in Shp2-D61G and 3055 ± 294 μm^2 in Shp2-A462T expressing embryos, compared to 3986 ± 398 μm^2 in WT-Shp2 expressing embryos; cf. Figure 6F). Importantly, treatment with 0.25 μM CI-1040 at 4.5 hpf rescued the counterclockwise rotation of the fluorescent beads in Shp2-D61G and Shp2-A462T expressing embryos to levels that were comparable to WT-Shp2 expressing embryos (Figure 6 J-M). Taken together, these results suggest that the cardiac defects in zebrafish embryos expressing NS and LS Shp2-variants are due to hyperactivate MAPK-induced laterality defects originating from impaired cilia function in KV.

Discussion

In this paper, we used zebrafish to investigate defects in cardiac development in response to expression of NS and LS variants of Shp2. We found that NS- and LS-Shp2 expressing embryos showed impaired leftward heart displacement. Our results are consistent with a report that Noonan-associated mutations induce a cardiac looping defect in *Xenopus* [47]. Here, we provide insight into the underlying mechanism. The cardiac defects that we observed in zebrafish embryos are associated with L/R laterality defects and with defects in ciliogenesis. Expression of NS and LS variants of Shp2 in zebrafish embryos enhanced MAPK activation. The laterality defects were rescued by early treatment with CI-1040, a MEK inhibitor, indicating that the defects in heart asymmetry were caused by enhanced MAPK signaling before gastrulation.

Here, we focused on the cardiac defects in embryos expressing NS and LS Shp2-variants. The heart defects only became evident during cardiac tube formation, the first asymmetric process that occurs in the zebrafish heart [33]. Normally, the cardiac tube is displaced to the left, but in embryos expressing NS and LS Shp2 variants, heart displacement was randomized (Figure 3). Cell movement analyses revealed a delay in cell movements, coupled with reduced cardiac tube rotation, resulting in morphologically abnormal hearts at 28 hpf (Figure 4). Cell tracking studies showed that loss of Nodal or BMP signaling leads to similar defects [39,40]. Nodal mutant embryos show reduced speed and directional movement of the cardiomyocytes, resulting in disruption of the leftward morphogenesis and cardiac cone rotation. Asymmetric *spaw* expression in the LPM is responsible for the correct displacement of the heart tube to the left [40,41]. In line with these

findings, we found that expression of *spaw* was randomized in embryos expressing NS and LS Shp2-variants, concomitantly with its downstream gene target *lft2*. As a consequence, left/right asymmetry was lost and leftward displacement of the heart in embryos expressing Shp2-D61G and Shp2-A462T was compromised. In addition, randomized *fabp* expression suggested that not only asymmetry of the heart, but also of the liver was impaired.

Left-right asymmetry is conserved across species and defects in left-right asymmetry are collectively called laterality disease [48]. The phenotype we observed in zebrafish embryos expressing NS and LS Shp2-variants was characterized by randomization of left/right asymmetry. It is noteworthy that laterality disease is frequently associated with congenital heart defects (CHD) [38]. Impaired left-right patterning can affect cardiac morphogenesis, resulting in defective septation and/or double outlet right ventricle (DORV) [38]. Cardiac defects associated with laterality diseases are also reported in Shp2-D61G knock-in mice. A proportion of the heterozygous Shp2-D61G mice displays septal defects and DORV [30]. However, laterality defects are not the only cause of septation defects or DORV. Other laterality defects were not reported in NS or LS Shp2 knock-in mice and laterality defects have not been commonly reported in human individuals with NS and LS. Hence, it remains to be determined whether laterality defects have a role in human NS and LS.

In zebrafish expressing NS and LS variants of Shp2, we found that the underlying mechanism for randomization of L/R asymmetry is likely impaired cilia function in the KV. Particularly cilia length and KV area were associated with Shp2 variant induced impaired fluid flow in KV and subsequent loss of asymmetry (Figure 6). It is well established that L/R asymmetry is mediated by cilia that generate fluid flow within the KV, resulting in expression of *spaw* in the left side of the LPM [49,50]. Laser-mediated ablation of KV randomises expression of *spaw* and *lft2* [50]. Moreover, shorter cilia result in perturbed intravesicular fluid flow, leading to loss of asymmetry in the heart, brain and viscera [51]. KV formation is completed by the 6-somites stage (12 hpf) [52,53] and the generation of the KV depends on the dorsal forerunner cells (DFCs) that are induced during the blastula period [54]. Defects in the specification, clustering or organisation of DFCs induce defective KV organogenesis and/or ciliogenesis [50,53]. Therefore, it will be interesting to investigate the role of the NS and LS Shp2 variants in DFC biology.

Shp2 is a well-known downstream factor in FGFR signaling [8]. It has been reported that FGFR1 signaling regulates cilia length in zebrafish. Morpholino (MO)-mediated knockdown of FGFR1 in zebrafish reduces cilia length in KV and perturbs directional fluid flow, thus impairing L/R patterning of the embryo [43]. That knockdown of FGFR1, a positive regulator of MAPK signaling, has similar effects as mutant Shp2-induced hyperactivation of MAPK appears to be contradictive. However, it is not uncommon that attenuation and activation of a signaling pathway have the same effect on developmental processes. Apparently, FGFR1 knockdown on the one hand and Shp2 variant mediated enhanced MAPK activation on the other have similar effects on cilia function in KV and both impair L/R asymmetry. Our results predict that ectopic activation of MAPK signaling for instance by overexpression of (activated) MAPK around gastrulation would induce laterality defects as well.

Defective ciliogenesis was observed in the KV of NS and LS-Shp2 expressing embryos. It remains to be determined whether ciliogenesis in other organs is affected in these embryos as well. It is noteworthy that deafness is associated with LS in human patients. Deafness is typically associated with defective cilia in the inner ear and future work should focus on ciliogenesis in organs other than KV in NS and LS Shp2-variant expressing zebrafish embryos.

The cardiac defects that were induced by expression of NS and LS Shp2-variants in zebrafish embryos were indistinguishable. MAPK activation was elevated at bud stage in response to expression of both Shp2-D61G (NS) as well as Shp2-A462T (LS) (Figure 7H), which might explain why we observed similar developmental defects at early stages. It is well established that NS-Shp2 mutations enhance MAPK activation, but LS-Shp2 often does not activate MAPK signaling. Nevertheless, it is not unprecedented that LS mutations induce defects that are associated with activation of MAPK signaling. Expression of LS-Shp2 mutants in *Drosophila* results in ectopic wing veins and a rough eye phenotype, characteristics of increased Erk activation. This gain-of-function phenotype is similar to that of NS-Shp2 transgenic flies [25,26]. Moreover, a recent study shows that induced pluripotent stem cells (iPSCs) from LS patient-derived fibroblasts display higher basal pERK levels compared to those of control iPSCs [55]. How the NS and LS variants of Shp2 would both activate MAPK signaling remains to be determined. Whereas catalytic activity of Shp2 is enhanced by the NS mutations, it is reduced by the LS mutations, indicating that MAPK activation is not directly affected by alterations in Shp2 catalytic activity. Rather, the NS and LS Shp2-variant induced defects may result from a phosphatase-independent function of Shp2. Alternatively, as suggested in a recent report, the LS-variants of SHP2 retain some catalytic activity and mediate GOF phenotypes, because they have an increased propensity for the open conformation. Thus, the LS variants bind upstream activators preferentially and stay in complex with their scaffolding adapters longer, thus prolonging specific substrate turnover [22], which in turn may lead to MAPK activation.

Whereas MAPK activation may be elevated by both NS and LS variants of Shp2, elevated PI3K/AKT signaling is exclusively associated with LS. Hyperactivation of AKT signaling in response to LS-Shp2 is responsible for HCM in mouse hearts [31,56,57]. We also observed elevated pAkt levels in response to LS-Shp2 in zebrafish embryos (Supplemental Figure 3), but we did not observe HCM in these embryos. The cardiac defects in embryos expressing NS and LS Shp2-variants were indistinguishable. Moreover, these heart defects were rescued by early treatment with the MEK inhibitor to a similar extent, indicating a causal role for elevated MAPK activation in the observed cardiac defects, independently of Akt signaling.

In summary, our data provide new insights into the role of pathogenic Shp2 variants in cardiac development. Expression of NS and LS Shp2-variants led to similar cardiac defects in zebrafish that were associated with impaired L/R asymmetry, resulting from impaired cilia function in KV. Treatment with a MEK inhibitor prior to gastrulation rescued cilia function, L/R asymmetry and heart displacement, suggesting a causal relation with enhanced MAPK signaling. No studies to date have examined the effect of NS and LS Shp2-variants on L/R asymmetry. Our paper opens a new prospective to understand how pathogenic SHP2 and downstream MAPK activation relates to cardiac development through its effects on L/R asymmetry.

Materials and Methods

Fish line

Zebrafish were maintained and the embryos were staged as previously described [58]. The *tg(myl7:GFP)* line was previously described [59]. All procedures involving experimental animals were approved by the local animal experiments committee and performed in compliance with local animal welfare laws, guidelines and policies, according to national and European law.

Constructs, RNA and injections.

The eGFP-peptide 2A-Shp2 construct was derived by PCR. 5′ capped sense mRNAs were synthesized using the mMessage mMachine kit (Ambion) and linearized plasmid DNA. mRNA injections were performed at the one-cell stage as described [60] using optimized amounts of mRNA (D61G=150pg, A465T=50pg, T73I=80pg G465A=100pg, WT-Shp2=150pg).

Immunoblotting

Zebrafish embryos (10hpf) were lysed in buffer containing 50 mM Tris, pH 7.5, 150 mM NaCl, 1 mM EDTA, 1 mM sodium orthovanadate, 1% Nonidet P-40, 0.1% sodium deoxycholate, protease inhibitor mixture (Complete Mini, Roche Diagnostics) and vanadate. Samples were run on SDS-PAGE gel (10%), transferred to PVDF membrane and stained with Coomassie Blue to verify equal loading. The blots were probed with antibodies specific for SHP2, Actin, pERK, ERK, pAKT, AKT (all Cell Signaling) and GFP (Torrey Pines). Detection was done using enhanced chemiluminescence (Thermo Scientific kit).

In situ Hybridization and Immunofluorescence Microscopy

In situ hybridizations were done essentially as described [61] using probes specific for, *myl7* [37], *vmhc* [62], *amhc* [63], *has2* [64], *lefty-2* [65], *southpaw* [41], *fabp*, *shh* [42].
For zebrafish immunohistochemistry, embryos were fixed in 4% DENT'S solution at 4°C, and subsequently blocked for 1 hour in PBS containing 5% lamb serum, 1% BSA, 1% DMSO, and 0.1% Triton-X. Embryos were incubated in mouse anti-acetylated Tubulin (1:500, Sigma) for 3 hours at RT. After extensive washing, embryos were incubated in goat anti-mouse Alexa Fluor 488. Embryos were flat-mounted in glycerol. Images were acquired using an SPE laser scanning confocal microscope. Confocal z-series images were assembled to present the sum of the focal planes; cilia length, cilia number and KV lumen area were manually measured using Image J software (http://rsb.info.nih.gov/ij/).

Pharmacological inhibition of MAPK signaling

To test the prevention of the NS/LS Shp2 mRNA phenotype, embryos injected with NS/LS Shp2 mRNA were incubated with 0,25 µM CI-1040 at 4.5 hpf or 10 hpf for 1 hour at 28.5°C in the dark.

Time-Lapse Imaging and Analysis

Embryos at the 22-somite stage were dechorionated and mounted in glass-bottom 6-well plates using 0.25% agarose in E3 embryo medium containing 16 mg/ml 3-amino benzoic acid ethylester to block contractile movements. Confocal imaging was performed using a spinning disc confocal laser scanning microscope with 20x magnification, acquiring stacks every 5 min. Embryos were kept at 28.5°C during recordings. ImageJ software (http://rsb.info.nih.gov/ij/) was used to generate time-lapse movies and for cell counting. Cell tracking was done using Volocity software (Improvision) followed by manual inspection of individual tracks generating quantification of

total speed (track length/time). Rotation was calculated by measuring the angle with the LR axis of four imaginary lines connecting four individual cells at the start and the end of the time-lapse (200 min). All statistical analyses were performed in Excel (Microsoft) using the two-tailed student's T-test.

KV fluid flow and cilia motility

Fluorescent beads (Polysciences) were injected into KV to visualize flow as described [50]. Bead flow was imaged at the 8- to 10-somite stage (SS) on a Leica AF7000 microscope (Leica Microsystems GmbH, Wetzlar, Germany) using a 63× water dipping objective and an Hamamatsu C9300-221 high speed CCD camera (Hamamatsu Photonics, Hamamatsu City, Japan) at 80 fps to record a 10 sec movie. Movies were generated using ImageJ software. Bead tracking was done using Volocity software (Improvision). For each embryo, four to five beads were tracked for a minimum of 50 frames of the movie and the average bead velocity was calculated.

High-speed imaging and analysis

2 dpf embryos were mounted in 0.25% agarose prepared in E3 medium embryonic medium with 16 mg/ml 3-amino benzoic acid ethylester. Embryonic hearts were imaged with a Hamamatsu C9300-221 high speed CCD camera (Hamamatsu Photonics, Hamamatsu City, Japan) at 150 fps mounted on a Leica AF7000 microscope (Leica Microsystems GmbH, Wetzlar, Germany) in a controlled temperature chamber (28.5°C) using Hokawo 2.1 imaging software (Hamamatsu Photonics GmbH, Herrsching am Ammersee, Germany). Image analysis was carried out with ImageJ (http://rsbweb.nih.gov/ij/). Statistical analysis and drawing of the box-whisker plot were carried out in Excel 2007 (Microsoft, Redmond, WA, USA).

Statistics

Cilia measurements were analyzed using the two-tailed student's t-test. Averages for controls and experimental were compared within each clutch of embryos. Results were considered significant when $p<0.05$ and results are expressed as mean ± standard error of the mean (p values * $p<0.05$, ** $p<0.01$, *** $p<0.001$).

Acknowledgements

This work was funded, in part, by a grant from the Research Council for Earth and Life Sciences (ALW 819.02.021) with financial aid from the Netherlands Organisation for Scientific Research (NWO) (to J.d.H.).

Author contributions

JdH conceived the project; MB and JdH designed the approach with help from FT, EN and JB; MB, JPO, FT and EN performed experiments; MB and JdH prepared the manuscript, which was edited by JPO, FT, EN and JB prior to submission.

References

1. Feng GS, Hui CC, Pawson T (1993) SH2-containing phosphotyrosine phosphatase as a target of protein-tyrosine kinases. Science 259: 1607-1611.
2. Freeman RM, Jr., Plutzky J, Neel BG (1992) Identification of a human src homology 2-containing protein-tyrosine-phosphatase: a putative homolog of Drosophila corkscrew. Proc Natl Acad Sci U S A 89: 11239-11243.
3. Chan RJ, Feng GS (2007) PTPN11 is the first identified proto-oncogene that encodes a tyrosine phosphatase. Blood 109: 862-867.
4. Tidyman WE, Rauen KA (2009) The RASopathies: developmental syndromes of Ras/MAPK pathway dysregulation. Curr Opin Genet Dev 19: 230-236.
5. Neel BG, Gu H, Pao L (2003) The 'Shp'ing news: SH2 domain-containing tyrosine phosphatases in cell signaling. Trends Biochem Sci 28: 284-293.
6. Feng GS (1999) Shp-2 tyrosine phosphatase: signaling one cell or many. Exp Cell Res 253: 47-54.
7. Van Vactor D, O'Reilly AM, Neel BG (1998) Genetic analysis of protein tyrosine phosphatases. Curr Opin Genet Dev 8: 112-126.
8. Neel BG, Tonks NK (1997) Protein tyrosine phosphatases in signal transduction. Curr Opin Cell Biol 9: 193-204.
9. Huyer G, Alexander DR (1999) Immune signalling: SHP-2 docks at multiple ports. Curr Biol 9: R129-132.
10. Qu CK (2000) The SHP-2 tyrosine phosphatase: signaling mechanisms and biological functions. Cell Res 10: 279-288.
11. Tartaglia M, Mehler EL, Goldberg R, Zampino G, Brunner HG, et al. (2001) Mutations in PTPN11, encoding the protein tyrosine phosphatase SHP-2, cause Noonan syndrome. Nat Genet 29: 465-468.
12. Digilio MC, Conti E, Sarkozy A, Mingarelli R, Dottorini T, et al. (2002) Grouping of multiple-lentigines/ LEOPARD and Noonan syndromes on the PTPN11 gene. Am J Hum Genet 71: 389-394.
13. Mendez HM, Opitz JM (1985) Noonan syndrome: a review. Am J Med Genet 21: 493-506.
14. Legius E, Schrander-Stumpel C, Schollen E, Pulles-Heintzberger C, Gewillig M, et al. (2002) PTPN11 mutations in LEOPARD syndrome. J Med Genet 39: 571-574.
15. Sarkozy A, Digilio MC, Dallapiccola B (2008) Leopard syndrome. Orphanet J Rare Dis 3: 13.
16. Allanson JE, Roberts AE (1993) Noonan Syndrome. In: Pagon RA, Adam MP, Bird TD, Dolan CR, Fong CT et al., editors. GeneReviews. Seattle (WA).
17. Keilhack H, David FS, McGregor M, Cantley LC, Neel BG (2005) Diverse biochemical properties of Shp2 mutants. Implications for disease phenotypes. J Biol Chem 280: 30984-30993.
18. Kontaridis MI, Swanson KD, David FS, Barford D, Neel BG (2006) PTPN11 (Shp2) mutations in LEOPARD syndrome have dominant negative, not activating, effects. J Biol Chem 281: 6785-6792.
19. Hof P, Pluskey S, Dhe-Paganon S, Eck MJ, Shoelson SE (1998) Crystal structure of the tyrosine phosphatase SHP-2. Cell 92: 441-450.
20. Nakamura T, Gulick J, Pratt R, Robbins J (2009) Noonan syndrome is associated with enhanced pERK activity, the repression of which can prevent craniofacial malformations. Proc Natl Acad Sci U S A 106: 15436-15441.
21. Hanna N, Montagner A, Lee WH, Miteva M, Vidal M, et al. (2006) Reduced phosphatase activity of SHP-2 in LEOPARD syndrome: consequences for PI3K binding on Gab1. FEBS Lett 580: 2477-2482.
22. Yu ZH, Xu J, Walls CD, Chen L, Zhang S, et al. (2013) Structural and mechanistic insights into LEOPARD syndrome-associated SHP2 mutations. J Biol Chem 288: 10472-10482.
23. Stewart RA, Sanda T, Widlund HR, Zhu S, Swanson KD, et al. (2010) Phosphatase-dependent and -independent functions of Shp2 in neural crest cells underlie LEOPARD syndrome pathogenesis. Dev Cell 18: 750-762.
24. Edouard T, Combier JP, Nedelec A, Bel-Vialar S, Metrich M, et al. (2010) Functional effects of PTPN11 (SHP2) mutations causing LEOPARD syndrome on epidermal growth factor-induced phosphoinositide 3-kinase/AKT/ glycogen synthase kinase 3beta signaling. Mol Cell Biol 30: 2498-2507.
25. Oishi K, Gaengel K, Krishnamoorthy S, Kamiya K, Kim IK, et al. (2006) Transgenic Drosophila models of Noonan syndrome causing PTPN11 gain-of-function mutations. Hum Mol Genet 15: 543-553.
26. Oishi K, Zhang H, Gault WJ, Wang CJ, Tan CC, et al. (2009) Phosphatase-defective LEOPARD syndrome mutations in PTPN11 gene have gain-of-function effects during Drosophila development. Hum Mol Genet 18: 193-201.
27. De Rocca Serra-Nedelec A, Edouard T, Treguer K, Tajan M, Araki T, et al. (2012) Noonan syndrome-causing SHP2 mutants inhibit insulin-like growth factor 1 release via growth hormone-induced ERK hyperactivation, which contributes to short stature. Proc Natl Acad Sci U S A 109: 4257-4262.
28. Yang W, Klaman LD, Chen B, Araki T, Harada H, et al. (2006) An Shp2/SFK/Ras/Erk signaling pathway controls trophoblast stem cell survival. Dev Cell 10: 317-327.
29. Tang TL, Freeman RM, Jr., O'Reilly AM, Neel BG, Sokol SY (1995) The SH2-containing protein-tyrosine phosphatase SH-PTP2 is required upstream of MAP kinase for early Xenopus development. Cell 80: 473-483.
30. Araki T, Mohi MG, Ismat FA, Bronson RT, Williams IR, et al. (2004) Mouse model of Noonan syndrome reveals cell type- and gene dosage-dependent effects of Ptpn11 mutation. Nat Med 10: 849-857.
31. Marin TM, Keith K, Davies B, Conner DA, Guha P, et al. (2011) Rapamycin reverses hypertrophic cardiomyopathy in a mouse model of LEOPARD syndrome-associated PTPN11 mutation. J Clin Invest 121: 1026-1043.
32. Jopling C, van Geemen D, den Hertog J (2007) Shp2 knockdown and Noonan/LEOPARD mutant Shp2-induced

gastrulation defects. PLoS Genet 3: e225.
33. Bakkers J (2011) Zebrafish as a model to study cardiac development and human cardiac disease. Cardiovasc Res 91: 279-288.
34. Lien CL, Harrison MR, Tuan TL, Starnes VA (2012) Heart repair and regeneration: recent insights from zebrafish studies. Wound Repair Regen 20: 638-646.
35. Kim JH, Lee SR, Li LH, Park HJ, Park JH, et al. (2011) High cleavage efficiency of a 2A peptide derived from porcine teschovirus-1 in human cell lines, zebrafish and mice. PLoS One 6: e18556.
36. Tessadori F, van Weerd JH, Burkhard SB, Verkerk AO, de Pater E, et al. (2012) Identification and functional characterization of cardiac pacemaker cells in zebrafish. PLoS One 7: e47644.
37. Yelon D, Horne SA, Stainier DY (1999) Restricted expression of cardiac myosin genes reveals regulated aspects of heart tube assembly in zebrafish. Dev Biol 214: 23-37.
38. Ramsdell AF (2005) Left-right asymmetry and congenital cardiac defects: getting to the heart of the matter in vertebrate left-right axis determination. Dev Biol 288: 1-20.
39. Smith KA, Chocron S, von der Hardt S, de Pater E, Soufan A, et al. (2008) Rotation and asymmetric development of the zebrafish heart requires directed migration of cardiac progenitor cells. Dev Cell 14: 287-297.
40. de Campos-Baptista MI, Holtzman NG, Yelon D, Schier AF (2008) Nodal signaling promotes the speed and directional movement of cardiomyocytes in zebrafish. Dev Dyn 237: 3624-3633.
41. Long S, Ahmad N, Rebagliati M (2003) The zebrafish nodal-related gene southpaw is required for visceral and diencephalic left-right asymmetry. Development 130: 2303-2316.
42. Krauss S, Concordet JP, Ingham PW (1993) A functionally conserved homolog of the Drosophila segment polarity gene hh is expressed in tissues with polarizing activity in zebrafish embryos. Cell 75: 1431-1444.
43. Neugebauer JM, Amack JD, Peterson AG, Bisgrove BW, Yost HJ (2009) FGF signalling during embryo development regulates cilia length in diverse epithelia. Nature 458: 651-654.
44. Liu DW, Hsu CH, Tsai SM, Hsiao CD, Wang WP (2011) A variant of fibroblast growth factor receptor 2 (Fgfr2) regulates left-right asymmetry in zebrafish. PLoS One 6: e21793.
45. Runtuwene V, van Eekelen M, Overvoorde J, Rehmann H, Yntema HG, et al. (2011) Noonan syndrome gain-of-function mutations in NRAS cause zebrafish gastrulation defects. Dis Model Mech 4: 393-399.
46. Anastasaki C, Estep AL, Marais R, Rauen KA, Patton EE (2009) Kinase-activating and kinase-impaired cardio-facio-cutaneous syndrome alleles have activity during zebrafish development and are sensitive to small molecule inhibitors. Hum Mol Genet 18: 2543-2554.
47. Langdon Y, Tandon P, Paden E, Duddy J, Taylor JM, et al. (2012) SHP-2 acts via ROCK to regulate the cardiac actin cytoskeleton. Development 139: 948-957.
48. Mercola M, Levin M (2001) Left-right asymmetry determination in vertebrates. Annu Rev Cell Dev Biol 17: 779-805.
49. Nonaka S, Tanaka Y, Okada Y, Takeda S, Harada A, et al. (1998) Randomization of left-right asymmetry due to loss of nodal cilia generating leftward flow of extraembryonic fluid in mice lacking KIF3B motor protein. Cell 95: 829-837.
50. Essner JJ, Amack JD, Nyholm MK, Harris EB, Yost HJ (2005) Kupffer's vesicle is a ciliated organ of asymmetry in the zebrafish embryo that initiates left-right development of the brain, heart and gut. Development 132: 1247-1260.
51. Ferrante MI, Romio L, Castro S, Collins JE, Goulding DA, et al. (2009) Convergent extension movements and ciliary function are mediated by ofd1, a zebrafish orthologue of the human oral-facial-digital type 1 syndrome gene. Hum Mol Genet 18: 289-303.
52. Oteiza P, Koppen M, Concha ML, Heisenberg CP (2008) Origin and shaping of the laterality organ in zebrafish. Development 135: 2807-2813.
53. Oteiza P, Koppen M, Krieg M, Pulgar E, Farias C, et al. (2010) Planar cell polarity signalling regulates cell adhesion properties in progenitors of the zebrafish laterality organ. Development 137: 3459-3468.
54. Alexander J, Rothenberg M, Henry GL, Stainier DY (1999) casanova plays an early and essential role in endoderm formation in zebrafish. Dev Biol 215: 343-357.
55. Carvajal-Vergara X, Sevilla A, D'Souza SL, Ang YS, Schaniel C, et al. (2010) Patient-specific induced pluripotent stem-cell-derived models of LEOPARD syndrome. Nature 465: 808-812.
56. Schramm C, Fine DM, Edwards MA, Reeb AN, Krenz M (2012) The PTPN11 loss-of-function mutation Q510E-Shp2 causes hypertrophic cardiomyopathy by dysregulating mTOR signaling. Am J Physiol Heart Circ Physiol 302: H231-243.
57. Ishida H, Kogaki S, Narita J, Ichimori H, Nawa N, et al. (2011) LEOPARD-type SHP2 mutant Gln510Glu attenuates cardiomyocyte differentiation and promotes cardiac hypertrophy via dysregulation of Akt/GSK-3beta/beta-catenin signaling. Am J Physiol Heart Circ Physiol 301: H1531-1539.
58. Kimmel CB, Ballard WW, Kimmel SR, Ullmann B, Schilling TF (1995) Stages of embryonic development of the zebrafish. Dev Dyn 203: 253-310.
59. Chocron S, Verhoeven MC, Rentzsch F, Hammerschmidt M, Bakkers J (2007) Zebrafish Bmp4 regulates left-right asymmetry at two distinct developmental time points. Dev Biol 305: 577-588.
60. Hyatt TM, Ekker SC (1999) Vectors and techniques for ectopic gene expression in zebrafish. Methods Cell Biol 59: 117-126.
61. Thisse C, Thisse B, Schilling TF, Postlethwait JH (1993) Structure of the zebrafish snail1 gene and its expression in

wild-type, spadetail and no tail mutant embryos. Development 119: 1203-1215.
62. Yelon D (2001) Cardiac patterning and morphogenesis in zebrafish. Dev Dyn 222: 552-563.
63. Smith KA, Joziasse IC, Chocron S, van Dinther M, Guryev V, et al. (2009) Dominant-negative ALK2 allele associates with congenital heart defects. Circulation 119: 3062-3069.
64. Bakkers J, Kramer C, Pothof J, Quaedvlieg NE, Spaink HP, et al. (2004) Has2 is required upstream of Rac1 to govern dorsal migration of lateral cells during zebrafish gastrulation. Development 131: 525-537.
65. Bisgrove BW, Essner JJ, Yost HJ (1999) Regulation of midline development by antagonism of lefty and nodal signaling. Development 126: 3253-3262.

Supplemental data

eGFP- peptide 2A- Shp2 fusions allow monitoring of expression of (mutant) Shp2.

In order to monitor injection efficiency, we fused an eGFP-peptide 2A sequence to the NH2-terminus of Shp2. The peptide 2A sequence in the fusion protein is cleaved autoproteolytically [35], producing eGFP and (mutant) Shp2 (Figure S1A), which was confirmed by immunoblotting (Figure S1B). Moreover, eGFP was readily visualized in the injected embryos at 48 hpf (Figure S1C,D). Injection of wild type Shp2 was used as a control and throughout this study Shp2-D61G was used as prototypical NS-variant and Shp2-A462T as LS-variant. Some of the experiments were done with additional variants with similar results. Morphological analysis of the embryos at 48 hpf indicated that injections of the GFP-peptide 2A-Shp2 fusions phenocopied the previously published phenotypes of NS-Shp2 and LS-Shp2, including short stature, craniofacial defects and cardiac defects [32]. (Figure S1C-D). Therefore, we used the GFP-peptide 2A-Shp2 fusions, monitored GFP expression and selected efficiently injected embryos for further analysis unless indicated otherwise.

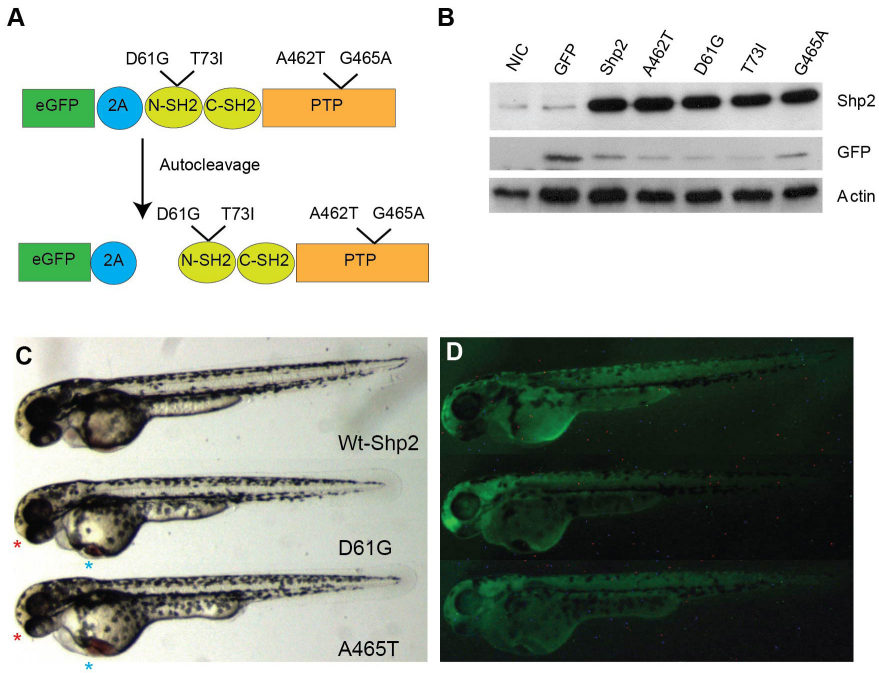

Supplemental Figure S1. EGFP-Peptide 2A-Shp2 fusions induced defects in zebrafish embryos. (A) Schematic representation of eGFP-Peptide 2A-Shp2 with D61G, T73I (NS) and A462T, G465A (LS) mutations indicated. The full length fusion protein is produced and is then cleaved autoproteolytically, resulting in eGFP and (mutant) Shp2. (B) One- or two-cell stage embryos were injected with in vitro transcribed mRNAs encoding the indicated proteins. Immunoblotting analysis reveals that autoproteolytic cleavage of the fusion proteins is highly efficient in zebrafish embryos. The injected embryos were lyzed at 10 hpf, proteins were separated on SDS-polyacrylamide gels, blotted and probed with antibodies specific for Shp2, GFP and β-actin as a loading control. (C-D) Two representative injected embryos (D61G and A462T) show craniofacial defects (red asterisks), a decrease in body length and cardiac edema (blue asterisks). These defects are absent in WT-Shp2 injected control embryos. Injection efficiency was checked by fluorescence microscopy with a GFP filter.

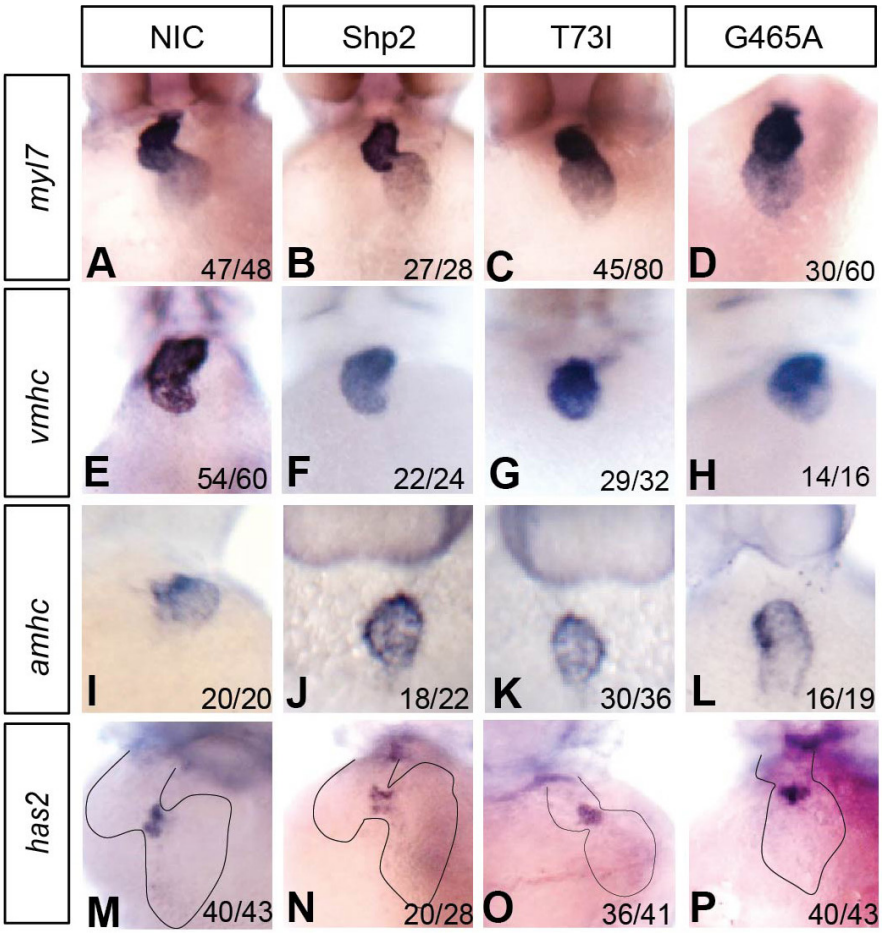

Supplemental Figure S2. Heart looping defects in embryos expressing Shp2-T73I (NS) and Shp2-G465A (LS). Non-injected control embryos (NIC) and embryos injected at the one-cell stage with mRNA encoding WT-Shp2, Shp2-T73I (NS) or Shp2-G465A (LS) were fixed at 48 hpf and *in situ* hybridization was performed using probes for the myosin genes *myl7* (A-D, cardiomyocytes), *vmhc* (E-H, ventricle), *amhc* (I-L, atrium), and for *has2* (M-P, endocardial cushions). Representative pictures are shown and the number of embryos showing this pattern as well as the total number of embryos that were analyzed is indicated in the bottom right corner of each panel. The outline of the heart is indicated with a dashed line in panels M-P.

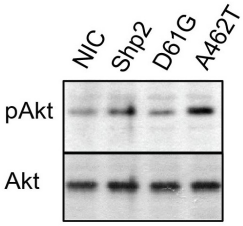

Supplemental Figure S3. Enhanced Akt signaling in Shp2-A462T (LS), but not Shp2-D61G (NS) expressing embryos. Zebrafish embryos were injected with WT-Shp2, Shp2-D61G (NS) or Shp2-A462T (LS) at the one-cell stage. Embryos were lysed at 10 hpf. Immunoblots of the zebrafish lysates were stained using antibodies specific for pAkt and Akt.

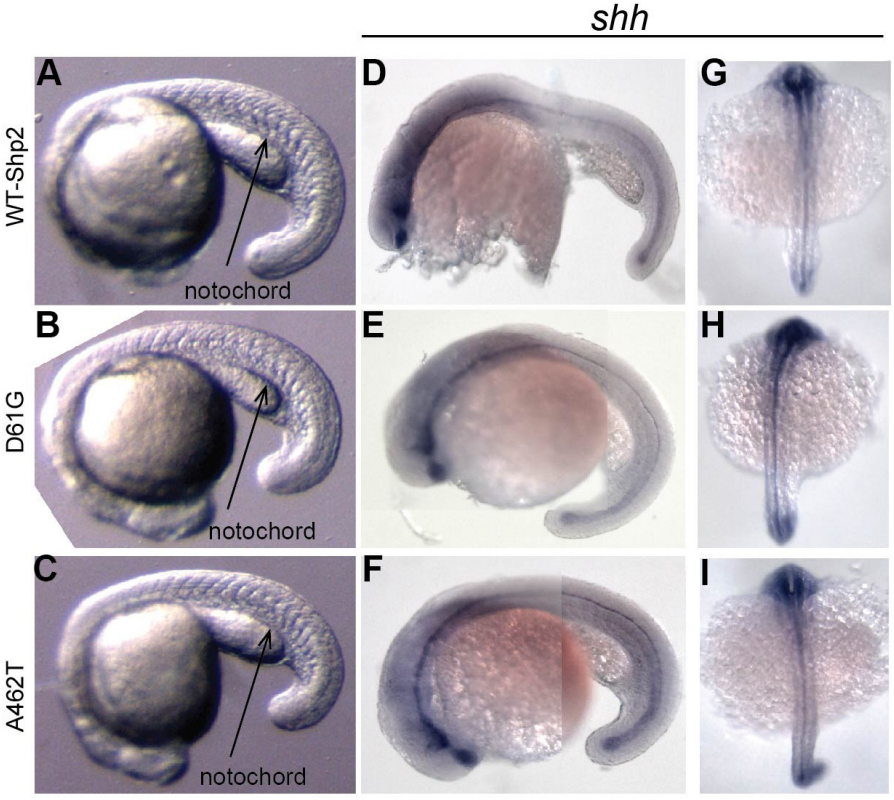

Supplemental Figure S4. Midline structures are intact in NS and LS Shp2-variants. Bright-field images of WT-Shp2 control (A) D61G (B) and A462T (C) embryos, showing normal notochord formation. (D-I) *In situ* hybridization analysis showed contiguous *shh* expression in the floorplate. The total number of embryos analyzed is: WT-Shp2, n=20/20; Shp2-D61G, n=30/30; Shp2-A462T, n=30/30.

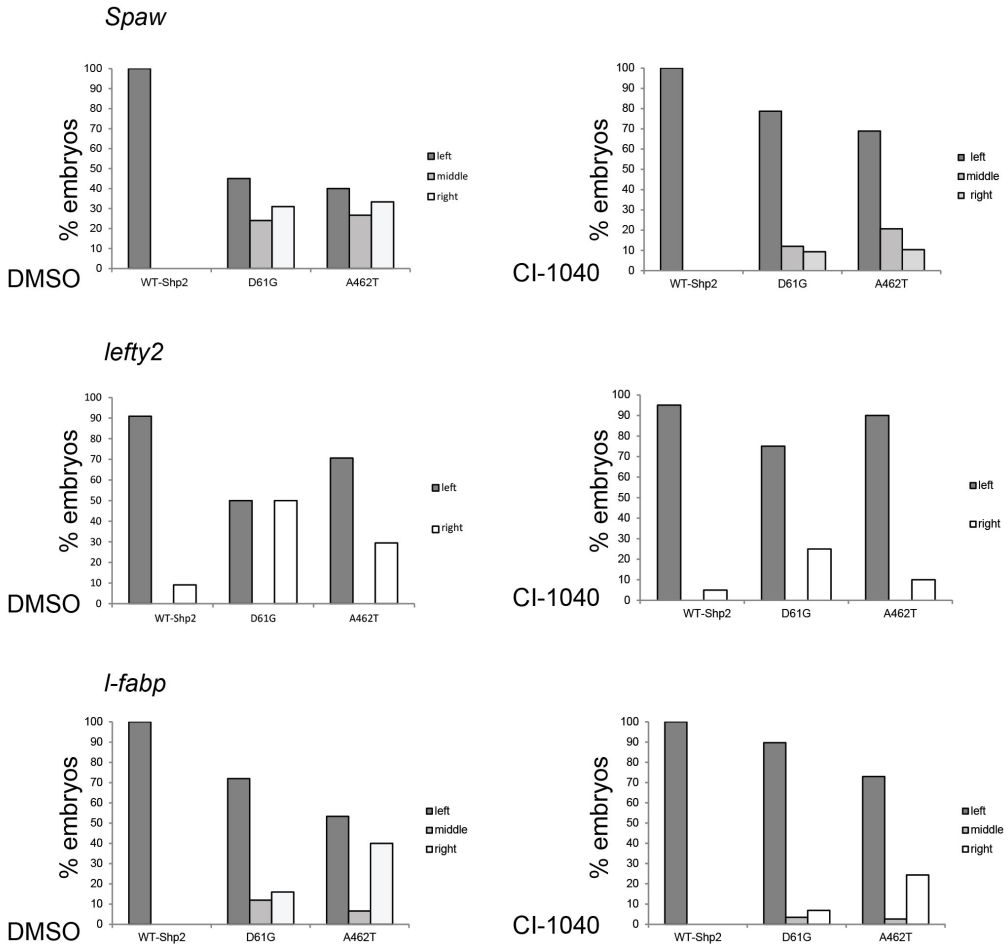

Supplemental Figure S5. Early treatment with the MEK-inhibitor, CI-1040, rescued L/R asymmetry in embryos expressing NS and LS Shp2-variants. Embryos were injected at the one-cell stage with mRNA encoding WT-Shp2 (Shp2), Shp2-D61G (NS) or Shp2-A462T (LS). Embryos were treated with MEK inhibitor CI-1040 (0.25 μM) for 1 h at 4.5 hpf or mock-treated with DMSO and fixed at the stage indicated in the panel. *In situ* hybridization was done using probes specific for *spaw* (A-B, *southpaw*), *lft2* (C-D, *lefty2*), and *fabp* (E-F, fatty acid binding protein, marking the liver). Markers asymmetry was scored for embryos injected with WT-Shp2, Shp2-D61G and Shp2-A462T. Percentages of left, middle/bilateral and right expression of the markers are depicted. The total number of embryos analyzed is: *spaw* (WT-Shp2 n=40, Shp2-D61G n=50, Shp2-A462T n=35); *lft2* (WT-Shp2 n=50, Shp2-D61G n=42, Shp2-A462T n=34) and *fabp* (WT-Shp2 n=26, Shp2-D61G n=28, Shp2-A462T n=35).